

Observation of size-independent effects in nanoparticle retention behavior during asymmetric-flow field-flow fractionation

Julien Gigault · Vincent A. Hackley

Received: 26 March 2013 / Revised: 4 May 2013 / Accepted: 7 May 2013 / Published online: 29 May 2013
© Springer-Verlag Berlin Heidelberg (outside the USA) 2013

Abstract In this work, we highlight the size-independent influence of the material properties of nanoparticles (NPs) on their retention behavior in asymmetric-flow field-flow fractionation (A4F) by comparing four NP populations with similar nominal size. The phenomena described here suggest there are limits to the effectiveness and accuracy of using a single type of NP standard (polystyrene beads most typically) in order to generically calibrate retention time in normal mode elution. The dual objectives of this paper are to (1) demonstrate the uncertainties resulting from current practice and (2) initiate a discussion of these effects and their origins. The results presented here illustrate clearly that the retention time is higher for metallic NPs relative to lower (bulk) density NPs. By modifying the fundamental field-flow fractionation equation to account for differences in particle density, we show that the effect of the gravitational force is finite but insignificant for NPs. We postulate that the observed material-dependent retention behavior may be attributed to differences in the attractive van der Waals force between the NPs and the accumulation wall (membrane surface). We hope that our results will stimulate discussion

and reassessment of the calibration procedure, perhaps by more fully accounting for all influential material parameters relevant to the fractionation of nanoscale particles by A4F.

Keywords Field-flow fractionation · Nanoparticles/nanotechnology · Separations/theory

Introduction

Field-flow fractionation (FFF), a single-phase chromatographic technique originally developed for separation of macromolecules by Giddings and coworkers [1], has been increasingly utilized in recent years to fractionate and characterize nanoscale and colloidal particles, including metals such as gold [2–4] and silver [5–9], carbon nanotubes [10–15], and polymers and proteins [16, 17]. Both manufactured and naturally occurring particles have been investigated [8, 18, 19]. Asymmetric-flow field-flow fractionation (A4F) is the most widely used and commercially available realization of FFF. A4F has demonstrated very high efficiency to fractionate and characterize particulate analytes according to physical parameters such as size and shape, and coupled with various on-line detectors, A4F can provide researchers with a powerful analytical tool with respect to on-line high-resolution multidimensional characterization and quantitative analysis [4, 10, 12, 20, 21]. Nevertheless, in FFF, a considerable complication exists in regard to the correct determination of the analyte diffusion coefficient, the principal determinant of retention time. There are obvious benefits to the use of on-line size measurements (e.g., using dynamic light scattering); however, such on-line measurements are sometimes limited due to the

Electronic supplementary material The online version of this article (doi:10.1007/s00216-013-7055-2) contains supplementary material, which is available to authorized users.

J. Gigault · V. A. Hackley (✉)
Materials Measurement Science Division,
National Institute of Standards and Technology,
100 Bureau Drive, Stop 8520,
Gaithersburg, MD 20899, USA
e-mail: vince.hackley@nist.gov

V. A. Hackley
e-mail: vincent.hackley@nist.gov

properties of the analyte (e.g., the optical properties, the size range, the dispersion state, and the shape heterogeneity). There are currently two approaches taken: (a) by using appropriate theoretical equations and inputting flow parameters known a priori, one can extract the diffusion coefficient (and thereby the hydrodynamic size) from the measured retention time or (b) by using standards certified in size to “calibrate” the retention time-size dependence for a specific set of flow conditions. Concerning the theoretical approach, some uncertainties may arise in terms of the elution process and a priori parameters. Uncertainties could arise by using incorrect values for void time, void volume, and the effective spacer (channel) thickness; these uncertainties are associated with both symmetric and asymmetric-flow FFF. The empirical method (i.e., use of calibration standards), while mitigating some of the uncertainties associated with flow parameters, presents different issues including the quality, size, shape, and nature of the calibration materials required for implementation. Traceable polystyrene latex (PSL) bead reference standards are commonly utilized for this purpose, regardless of the target analyte composition [22, 23].

Generally, for the two different approaches highlighted above, the influence of material characteristics associated with the analyte and/or calibrants (e.g., core density, physical form) on the separation process has not been previously considered. Equations that govern the fractionation process in FFF operate under the assumption that the nature of the analyte has no significant effect on retention in the channel. In the case of analytes with bulk density close to 1 g cm^{-3} (e.g., many polymeric lattices, macromolecules), the equations can be effectively applied. Nevertheless, with the recent emergence of nanoscale particles having many different forms and compositions, including hybrid materials, a question arises as to the adequacy of the existing equations and calibration procedures for these materially variant analytes. For these reasons, the aim of the present work is to demonstrate influences on retention behavior arising from inherent material properties. This influence is experimentally demonstrated in the present work and discussed by theoretically calculating the influence of the particle nature on the retention time. However, a definitive explanation for the observed differences in retention behavior remains elusive and is an active research area for the authors.

Experimental section

Test materials

Citrate stabilized nominally 100-nm-diameter Au nanoparticles (AuNPs) and AgNPs in aqueous solution were obtained from

Ted Pella, Inc. (Redding, CA).¹ Nominally, 100 nm PSL (3100A, NIST-traceable Thermo Scientific Nanosphere Size Standard) was purchased from Fisher Scientific (Pittsburg, PA). SeNPs were synthesized by ascorbic acid reduction of Na_2SeO_3 and using sodium dodecyl sulfate (SDS) as the stabilizing agent. Briefly, to 8 mL of 60 mmol L^{-1} ascorbic acid in a glass vial was added 1 mL of 80 mmol L^{-1} SDS solution followed by vigorous stirring at room temperature. Finally, 1 mL of 20 mmol L^{-1} Na_2SeO_3 solution was rapidly added dropwise with continuous vigorous stirring at room temperature. After approximately 5 min, a red/orange color appears indicating the presence of SeNPs. The solution was then purified using stirred cell ultrafiltration at 100 kDa to remove excess reagents and dissolved species. Reagents used in this study are identified in the [Electronic Supplementary Material \(ESM\)](#). A nominal size of 100 nm was chosen for this study due to the convenience of obtaining and/or synthesizing four different compositions with the same size and spherical morphology, and due to the increasing importance of surface interactions in the nanosize regime.

Sample preparation

All samples were diluted in deionized water in the same manner in order to yield identical NP mass concentrations as injected into the fractionation channel; we previously established that particle concentration does not significantly affect the retention time over the range investigated in the present study (for details, see [Electronic Supplementary Material section 2](#) and [Fig. S2](#)).

Instrumentation

The flow-mode analysis system used in this investigation consists of an Eclipse 3+ A4F (Wyatt Technology, Santa Barbara, CA), a UV-vis absorbance diode array detector (DAD, 1200 series, Agilent Technologies, Santa Clara, CA), a multi-angle laser light scattering (MALS) detector (DAWN HELEOS, Wyatt Technology), and a dynamic light scattering (DLS) detector (DynaPro, Wyatt Technology). Data from the above detectors were collected and analyzed using Astra software version 5.3.1.18 (Wyatt Technology). The A4F channel height was established using a 250- μm spacer (optimized according to the NP size range—see [Table S1](#) in [ESM](#)). The trapezoidal channel geometry has dimensions as follows: 26.5 cm long and narrowing in width from 2.1 to 0.6 cm, for the 250- μm spacer. Precut polyethersulfone 10-kDa membranes were purchased from Wyatt Technology and used in the A4F cell. Mobile phase

¹ The identification of any commercial product or trade name does not imply endorsement or recommendation by the National Institute of Standards and Technology.

flow is generated using an isocratic pump (1100 series, Agilent Technologies) equipped with a degasser (Gastorr TG-14, Flom Co., Ltd., Tokyo, Japan). Injections are performed using a manual injection valve (Rheodyne 7725i, IDEX Corporation, Oak Harbor, WA) equipped with stainless steel sample loops of different volumes. The A4F and associated detection chain is coupled to a model 7700x inductively coupled plasma mass spectrometer (ICP)-MS (Agilent Technologies) with a Micro Mist nebulizer for quantitative mass determination. Off-line (batch mode) UV-vis absorbance and DLS measurements were performed using a PerkinElmer (Waltham, MA) Lambda 750 spectrometer and a Malvern Instruments Inc. (Westborough, MA) ZetaSizer Nano, respectively.

Measurements

On-line DLS and MALS measurements were conducted in a cell maintained at 20 ± 0.1 °C. Eluting samples were subject to ambient temperatures outside of the MALS cell, where the ambient temperature was generally within 2 °C of the experimental temperature. Discrete measurement results are reported as the mean with an associated uncertainty of one standard deviation (presented as an interval or error bar) based on typically three to five replicates performed under repeatability conditions. A4F traces represent the mean of three to five replicate injections, where the mean coefficient of variation for the retention time between replicate elutions is typically less than 1 %. The mobile phase contained 0.5 mmol L^{-1} of ammonium nitrate (NH_4NO_3) filtered at $0.1 \mu\text{m}$ in order to remove any particulate impurities. This mobile phase was optimized in order to achieve the highest possible recovery (>88 %) for each of the four nanomaterials eluted separately. Recovery in this mobile phase, under the experimental conditions used in this study, yielded values close to 100 % when eluted after focusing but without application of the cross-flow field.

Coupling between the A4F fractionation-detection train and the ICP-MS consists of a direct connection of the eluent exiting the MALS/DLS module to the ICP-MS nebulizer, with a flow rate adjusted to maintain constant pressure inside the A4F channel. In this study, ICP-MS was operated without the collision cell, because of the lack of interference for the three mass isotopes of interest (^{107}Ag , ^{197}Au , and ^{77}Se). The calibration of the ICP-MS was realized by placement of a six-way injection valve (Rheodyne 7725i, IDEX Corporation) with a $100\text{-}\mu\text{L}$ stainless steel sample loop between the MALS/DLS detector and the entrance of the ICP-MS nebulizer. For the calibration of the coupled A4F-DAD-MALS/DLS-ICP-MS, elemental standard solutions (in 2 % mass fraction of nitric acid) of various concentrations were injected ($20 \mu\text{L}$) and replicated in order to have an accurate elemental (Au, Ag, and Se) mass quantification.

All other relevant instrument parameters and performance conditions used for A4F and ICP-MS are summarized in Table S1 of the Electronic Supplementary Material.

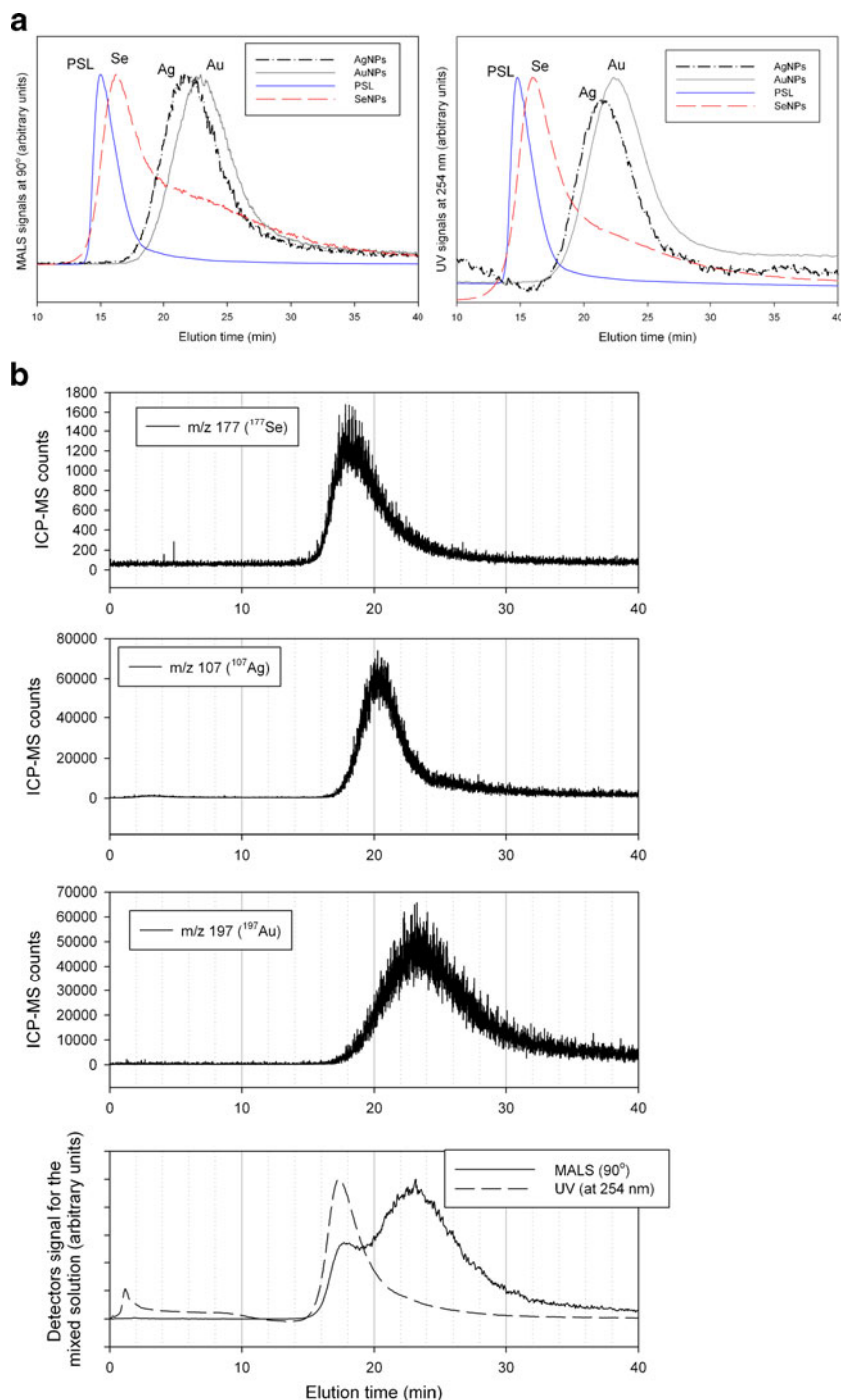
Results and discussion

In this study, nominally 100-nm-diameter particles of PSL, Se, Ag, and Au were analyzed. All samples were initially characterized off-line by DLS. The calculated intensity-weighted hydrodynamic size distributions are presented in Fig. S3 of the Electronic Supplementary Material. The zeta potential measured under conditions used for the A4F injection (calculated from electrophoretic mobility using the Smoluchowski limit) is reported in Table S2 of the Electronic Supplementary Material (as is the core density used for each material). The mean size obtained was 100 ± 7 nm for the four NP populations, but note that for Au and Ag, the size distribution is broader compared with Se and especially PSL. Additionally, it should be noted that each of the four populations yielded a negative zeta potential, with a mean magnitude of -39 ± 1 mV, which can be considered essentially equivalent (suggesting that interparticle and particle-membrane electrostatic forces will be almost identical).

Figure 1a presents fractograms realized with previously optimized conditions (see also Table S1 in the Electronic Supplementary Material) for the four negatively charged nominally 100-nm NP populations. The results exhibit differences in peak shape but also, most notably, in the retention time. For Ag and Au, the peaks obtained are broader than those obtained for PSL and Se; this can be attributed to the broader dispersion observed independently in the hydrodynamic diameter measured off-line (Fig. S1 in the Electronic Supplementary Material).

For the same size, it appears that the retention time increases with the bulk or core density of the NPs. The four NP populations were then combined and analyzed in mixed form in order to test if the observed influence remained. By coupling A4F with ICP-MS, it is possible to monitor the single-element NPs (Se, Ag, and Au), and by coupling with the DAD set to 254 nm and the MALS detector, it is possible to observe the PSL signal in the mixture at early elution time (below 20 min). Figure 1b shows the three distinct ICP-MS signals obtained from the mixture and corresponding to the Se, Ag, and Au NPs eluting at different times in order of their core density, and corresponding closely with the results obtained on individually injected samples. This result demonstrates that the nature of the nanoscale particles (exclusive of their size) influences their retention. Figure 2 plots the peak maximum retention time measured for each NP population versus the NP core density.

Fig. 1 **a** Representative UV and MALS fractograms for the four different NPs analyzed separately; **b** ICP-MS and UV fractograms for a mixture of the four NPs



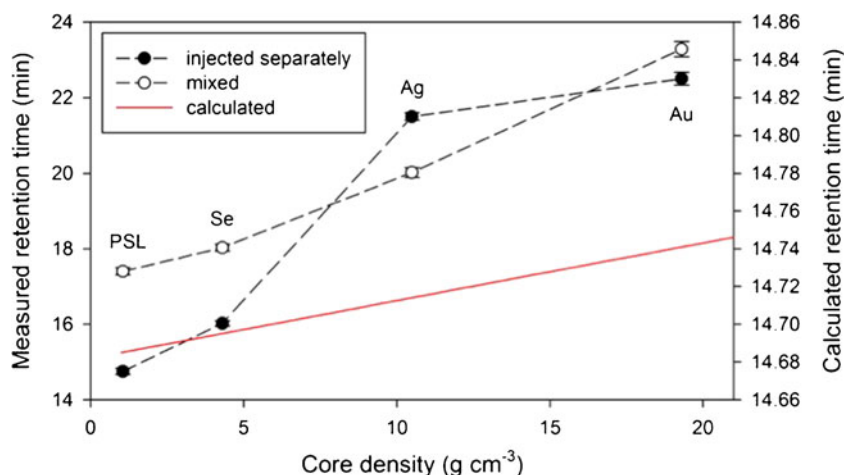
In order to test if the observed retention differences are truly related to the NP core density, we tried two different approaches. First, we modified the basic equation for FFF by introducing a term to account for the gravitational force. In flow FFF, the retention parameter λ defines the distance between the accumulation wall and the center of gravity of the eluting NP zone

relative to the channel thickness (previously determined) and is expressed as [11]:

$$\lambda = \frac{kT}{F\omega} \quad (1)$$

where k is the Boltzmann constant, T is the absolute

Fig. 2 Plots of the measured retention time as a function of NP core density (injected separately or mixed together) and the theoretically calculated relationship (red dashed line, right y-axis) obtained by applying the modified Eq. (6) described in the text



temperature, ω is the channel thickness, and F is the transverse force applied inside the channel.

In classical flow FFF, F arises from the applied cross flow and is expressed as:

$$F = F_x = 3\pi\eta d_p U \tag{2}$$

where $U = \frac{V_c}{V^0} \omega$ is the longitudinal velocity (dependent on the cross-flow rate V_c , void volume V^0 , and channel thickness ω) in the channel, η is the viscosity of the mobile phase, and d_p is the analyte hydrodynamic diameter. By taking account of the force due to gravity F_g (depending on the core density of the particles), it is possible to rewrite Eq. (2) as such:

$$F = F_x + F_g \tag{3}$$

where

$$F_g = \frac{\pi}{6} d_p^3 (\rho - \rho_0) g \tag{4}$$

and $(\rho - \rho_0)$ is the density differential between the analyte and the mobile phase (using the density for water), and g is the gravitational constant. In the case of long retention times in normal mode elution ($\lambda < 0.01$), the retention ratio for spheres can be approximated as [11]:

$$R = 6\lambda \tag{5}$$

where

$$R = \frac{t_0}{t_R}$$

where t_0 and t_R are the void time and analyte retention time, respectively, as they are defined in the literature [1]. With these relationships, it is then possible to link retention time with both NP size and density, such that:

$$R = \frac{6kT}{\omega\pi \frac{1}{6} d^3 g \Delta\rho + 3\pi\eta d \frac{1}{V^0} \dot{V}_c \omega^2} \tag{6}$$

By plotting the calculated retention time against the density of the analyte core (Fig. 2, solid red line), one observes a theoretical relationship that generally follows the upward trend observed experimentally, but which is substantially below the magnitude of the experimentally observed dependence. So the theoretical influence of core density would appear to be sufficiently small to ignore for all practical purposes.

Next, we considered that any influence of NP density should be mitigated simply by inverting the channel such that the gravitational force opposes the cross-flow force. This simple experiment was performed (see Electronic Supplementary Material, Fig. S4), and we observed that the retention time does in fact slightly decrease for the same analyte. The experiment was repeated several times using different orientations, and with consistent results. Yet, the observed shift due to orientation, though reproducible, is very small in magnitude. So core density alone cannot explain the observed differences in retention between the four NP samples. Neither can these differences easily be attributed to surface charge effects, as zeta potential measurements indicate that all four species have similar electrostatic characteristics.

It is worth noting that NPs injected separately, with the exception of Ag, exhibit a slower elution relative to individually injected populations. For NPs injected separately, the concentration profile of the population is not influenced by the presence of other species during elution. But for the mixed NP sample, the four population profiles overlap due to their size regime. The result suggests that the presence of NPs containing different core materials somehow influences (retards) the elution process, at least for the lower density

PSL and Se. However, a clear mechanistic explanation for this phenomenon is not obvious.

To summarize, the experimental results show an apparent substantial dependency of retention on the NP core density; however, a simple modification of the flow FFF equation based on additivity of the cross flow and gravitational forces clearly fails to account for the full magnitude of the observed dependency. On the other hand, inclusion of the gravitational force does qualitatively follow the experimental results (i.e., retention increases with core density, as one might expect).

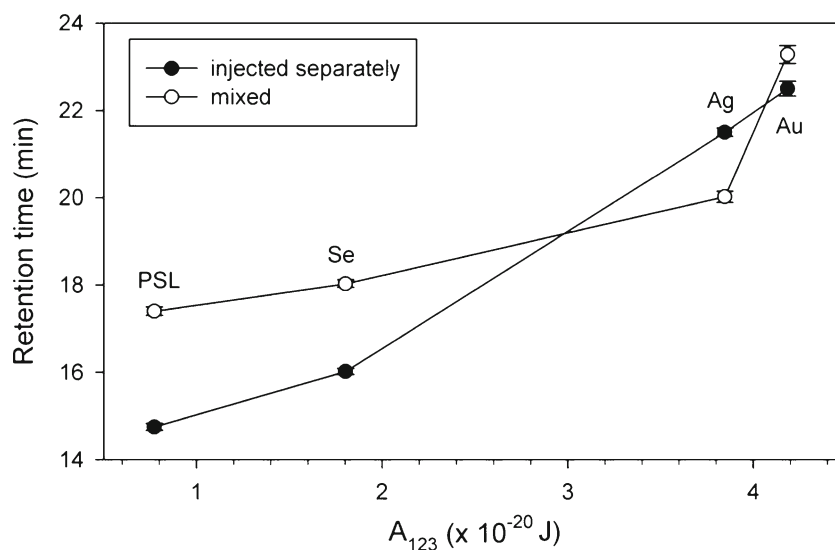
We therefore propose a second mechanism that we believe can account for the observed material dependence of retention behavior, one that is posited on differences in the attractive component of the DLVO interaction forces acting between the NPs and the membrane surface (and secondarily between the NPs themselves). Given that the electrostatic component is essentially a constant in this system, the material-dependent attractive component can be considered exclusively and compared for the four NP populations used in the study (while the authors concede that the totality of the interaction force–distance curve must also consider the electrostatic, and possibly a steric, component). The Hamaker constant reflects the intermolecular dipole interactions that cumulatively determine the van der Waals (VdW) attractive force between two bodies of matter in close proximity (10 nm or less). The magnitude of the effective Hamaker constant (A_{123}) depends on the polarizability of the two bodies (1 and 3) interacting through an intervening dielectric medium (in this case, water, 2). It can be shown (see Electronic Supplementary Material section 5) that the VdW interaction energy, V_{VdW} , for a sphere at a planar surface, an appropriate model for A4F, is directly proportional to both the effective

Hamaker constant and the particle size (and inversely proportional to the distance between the two surfaces) [24]. Since size is nominally constant in our system, the VdW force is then directly proportional to A_{123} , which, as it turns out, correlates strongly with the core density of the NPs (Fig. 3). Furthermore, for any two interacting materials, V_{VdW} for a sphere-on-planar geometry is approximately two times that for the corresponding sphere–sphere interaction.

It is worth noting that the difference in retention time for NPs injected separately (single component) versus mixed (multicomponent) increases as the Hamaker constant decreases (the exception being Ag). This suggests that in addition to the influence of the van der Waals attractive force on the interaction between the NPs and the membrane surface, there is also an influence resulting from the interaction between the different components in the mixture. In this case, the presence of NPs with relatively high values of A_{11} (Au, Ag), and stronger interaction with the membrane surface, may in effect retard the elution of NPs that otherwise would have a weaker interaction with the membrane and thus elute faster. Simply stated, PSL NPs elute more slowly in the presence of AuNPs of similar size. This is not likely attributable to the increased particle concentration in the mixed system, since the PSL particles far outnumber the AuNPs, and as previously stated, the effect of concentration alone on retention does not appear to be significant in the range tested here.

Even if some uncertainties remain regarding the underlying factors determining the apparent core density dependence of the retention behavior, it is clear from this work that judicious selection of calibrants must be made in order to extract accurate size data based solely on retention times for specific nanoscale analytes. Our hypothesis is that the surface structures and interfacial chemistry (i.e., bound

Fig. 3 Correlation between A4F retention and the van der Waals attractive energy of interaction, where the latter is represented by the effective 3-body Hamaker constant for each NP population at a polymer membrane surface with an intervening medium consisting of water



ligands, structural irregularities or asymmetries, hydrophilicity, etc.) of the NPs can also contribute to the complexity of their separation behavior, making a quantitative evaluation based solely on retention time challenging, to say the least.

Ongoing studies endeavor to interrogate other material factors in order to more fully evaluate the observed retention phenomena for nanoscale particles. Nevertheless, as the zeta potentials determined for the four NP populations in this study are quite similar, this suggests that the observed differences cannot be easily attributed to surface charge-related effects. Similarly, the contribution of the surface-bound stabilizers (i.e., SDS, citrate) to the effective hydrodynamic size of the particles is insignificant compared to their nominal core size (in the present case) and thus not likely to differentially impact retention. The VdW interaction force seems to us to be the most likely explanation, at least qualitatively.

Conclusions

In this work, we have demonstrated a clear influence of the core NP material nature on the retention process in the A4F channel, using several complementary detectors. Through these reproducible results, we show that retention time increases for nominally size-matched metallic NPs compared to lower density PSL and Se NPs. Even though these observed deviations in retention time follow the same tendency predicted by taking account of the particle core density in the flow FFF equation, the calculated effect of density alone is very small. A comparison of the material-dependent van der Waals interaction forces between spherical particles and a planar surface appear, at least qualitatively, to explain the observed dependence. It is hoped that the present work will stimulate further interest and discussion within the analytical community regarding the calibration of FFF and the influence of material properties on retention behavior, particularly in complex mixtures of NP populations. It is worth noting that although the use of on-line size detection can be extremely beneficial in the context of the present study, it is often limited by the material properties and conditions of the experiment (see Electronic Supplementary Material section 6 and Fig. S5). For example, DLS becomes increasingly ineffective when the particle size approaches or exceeds ≈ 100 nm, due to the difficulty of accurately measuring autocorrelation decays for more slowly diffusing particles in a flow-cell configuration. Similarly, the strong optical absorbance associated with some metal NPs yields MALS data that are not conducive to Zimm plot analysis. The standardization of A4F therefore remains a significant analytical

challenge for NP characterization, creating also many opportunities for research.

Acknowledgments The authors thank Prof. Michel Martin of ESPCI ParisTech and Dr. John Pettibone of NIST for helpful comments and suggestions regarding this work.

References

- Schimpf ME, Caldwell K, Giddings JC (2000) Field-flow fractionation handbook. Wiley, New York
- Calzolari L, Gilliland D, Garcia CP, Rossi F (2011) Separation and characterization of gold nanoparticle mixtures by flow-field-flow fractionation. *J Chromatogr A* 1218(27):4234–4239
- Cho TJ, Hackley VA (2010) Fractionation and characterization of gold nanoparticles in aqueous solution: asymmetric-flow field flow fractionation with MALS, DLS, and UV–vis detection. *Anal Bioanal Chem* 398(5):2003–2018. doi:10.1007/s00216-010-4133-6
- Gigault J, Cho TJ, MacCuspie RI, Hackley VA (2013) Gold nanorod separation and characterization by asymmetric-flow field flow fractionation with UV–vis detection. *Anal Bioanal Chem* 405:1191–202
- Bolea E, Jiménez-Lamana J, Laborda F, Castillo JR (2011) Size characterization and quantification of silver nanoparticles by asymmetric flow field-flow fractionation coupled with inductively coupled plasma mass spectrometry. *Anal Bioanal Chem* 401(9):2723–2732. doi:10.1007/s00216-011-5201-2
- Hagendorfer H, Kaegi R, Parlinska M, Sinnet B, Ludwig C, Ulrich A (2012) Characterization of silver nanoparticle products using asymmetric flow field flow fractionation with a multidetector approach—a comparison to transmission electron microscopy and batch dynamic light scattering. *Anal Chem* 84(6):2678–2685
- Poda AR, Bednar AJ, Kennedy AJ, Harmon A, Hull M, Mitrano DM, Ranville JF, Steevens J (2011) Characterization of silver nanoparticles using flow-field flow fractionation interfaced to inductively coupled plasma mass spectrometry. *J Chromatogr A* 1218(27):4219–4225. doi:10.1016/j.chroma.2010.12.076
- Gigault J, Hackley VA (2012) Differentiation and characterization of isotopically modified silver nanoparticles in aqueous media using asymmetric-flow field flow fractionation coupled to optical detection and mass spectrometry. *Anal Chim Acta*. doi:10.1016/j.aca.2012.11.060
- Pettibone JM, Gigault J, Hackley VA (2013) Discriminating the states of matter in metallic nanoparticle transformations: what are we missing? *ACS Nano* 7(3):2491–2499
- Chun J, Fagan JA, Hobbie EK, Bauer BJ (2008) Size separation of single-wall carbon nanotubes by flow-field flow fractionation. *Anal Chem* 80(7):2514–2523. doi:10.1021/ac7023624
- Gigault J, Grassl B, Lespes G (2011) Multi-wall carbon nanotube aqueous dispersion monitoring by using A4F-UV-MALS. *Anal Bioanal Chem* 401(10):3345–3353
- Gigault J, Grassl B, Lespes G (2012) A new analytical approach based on asymmetrical flow field-flow fractionation coupled to ultraviolet spectrometry and light scattering detection for SWCNT aqueous dispersion studies. *Analyst* 137(4):917–923
- Gigault J, Le Hécho I, Dubascoux S, Potin-Gautier M, Lespes G (2010) Single walled carbon nanotube length determination by asymmetrical-flow field-flow fractionation hyphenated to multi-angle laser-light scattering. *J Chromatogr A* 1217(50):7891–7897. doi:10.1016/j.chroma.2010.10.042
- Isaacson CW, Bouchard D (2010) Asymmetric flow field flow fractionation of aqueous C60 nanoparticles with size determination

- by dynamic light scattering and quantification by liquid chromatography atmospheric pressure photo-ionization mass spectrometry. *J Chromatogr A* 1217(9):1506–1512. doi:10.1016/j.chroma.2009.12.060
15. Tagmatarchis N, Zattoni A, Reschiglian P, Prato M (2005) Separation and purification of functionalised water-soluble multi-walled carbon nanotubes by flow field-flow fractionation. *Carbon* 43(9):1984–1989. doi:10.1016/j.carbon.2005.03.011
 16. Jungmann N, Schmidt M, Maskos M (2001) Characterization of polyorganosiloxane nanoparticles in aqueous dispersion by asymmetrical flow field-flow fractionation. *Macromolecules* 34(23):8347–8353. doi:10.1021/ma0106752
 17. Schultes S, Mathis K, Zillies J, Zwirock K, Coester C, Winter G (2009) Analysis of polymers and protein nanoparticles using asymmetrical flow field-flow fractionation (AF4). *LC-GC Eur* 22(8):390–403
 18. Baalousha M, Stolpe B, Lead JR (2011) Flow field-flow fractionation for the analysis and characterization of natural colloids and manufactured nanoparticles in environmental systems: a critical review. *J Chromatogr A* 1218(27):4078–4103. doi:10.1016/j.chroma.2011.04.063
 19. Delay M, Frimmel FH (2012) Nanoparticles in aquatic systems. *Anal Bioanal Chem* 402(2):583–592
 20. Hagendorfer H, Kaegi R, Traber J, Mertens SF, Scherrers R, Ludwig C, Ulrich A (2011) Application of an asymmetric flow field flow fractionation multi-detector approach for metallic engineered nanoparticle characterization—prospects and limitations demonstrated on Au nanoparticles. *Anal Chim Acta* 706(2):367–378. doi:10.1016/j.aca.2011.08.014
 21. Lespes G, Gigault J (2011) Hyphenated analytical techniques for multidimensional characterisation of submicron particles: a review. *Anal Chim Acta* 692(1–2):26–41
 22. Bouby M, Geckeis H, Geyer FW (2008) Application of asymmetric flow field-flow fractionation (AsFFFF) coupled to inductively coupled plasma mass spectrometry (ICPMS) to the quantitative characterization of natural colloids and synthetic nanoparticles. *Anal Bioanal Chem* 392(7–8):1447–1457. doi:10.1007/s00216-008-2422-0
 23. Dubascoux S, Le Hécho I, Potin Gautier M, Lespes G (2008) On-line and off-line quantification of trace elements associated to colloids by As-FI-FFF and ICP-MS. *Talanta* 77(1):60–65
 24. Brant JA, Childress AE (2002) Assessing short-range membrane-colloid interactions using surface energetics. *J Membr Sci* 203(1–2):257–273